Supramolecular Polymers in Aqueous Medium: Rational Design Based on Directional Hydrophobic Interactions

Alona Ustinov,[†] Haim Weissman,[†] Elijah Shirman,[†] Iddo Pinkas,[‡] Xiaobing Zuo,[§] and Boris Rybtchinski[*,†]

Departments of [†]Organic Chemistry and [‡]Plant Sciences, Weizmann Institute of Science, Rehovot 76100, Israel
[§]Argonne National Laboratory, 9700 South Cass Avenue, Argonne, Illinois 60439, United States

S *Supporting Information*

ABSTRACT: Self-assembly in aqueous medium is of primary importance and widely employs hydrophobic interactions. Yet, unlike directional hydrogen bonds, hydrophobic interactions lack directionality, making difficult rational self-assembly design. Directional hydrophobic motif would significantly enhance rational design in aqueous self-assembly, yet general approaches to such interactions are currently lacking. Here, we show that pairwise directional hydrophobic/π-stacking interactions can be designed using well-defined sterics and supramolecular multivalency. Our system utilizes a hexasubstituted benzene scaffold decorated with 3 (compound **1**) or 6 (compound **2**) amphiphilc perylene diimides. It imposes a pairwise self-assembly mode, leading to well-defined supramolecular polymers in aqueous medium. the assemblies were characterized using cryogenic electron microscopy, small-angle X-ray scattering, optical spectroscopy, and EPR. Supramolecular polymerization studies in the case of **2** revealed association constants in 10^8 M^{-1} range, and significant enthalpic contribution to the polymerization free energy. The pairwise PDI motif enables exciton confinement and localized emission in the polymers based on **1** and **2**'s unique photonic behavior, untypical of the extended π-stacked systems. Directional pairwise hydrophobic interactions introduce a novel strategy for rational design of noncovalent assemblies in aqueous medium, and bring about a unique photofunction.
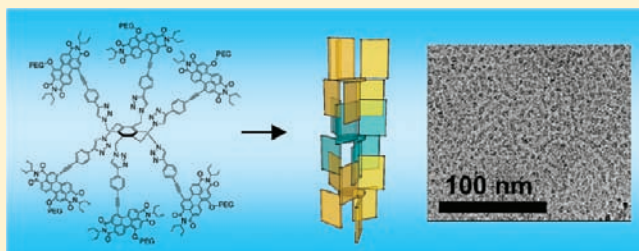
INTRODUCTION

Supramolecular chemistry employs noncovalent interactions between molecular building blocks in order to construct nanoscale architectures.[1−4] While some of these interactions (e.g., hydrogen bonds) exhibit strong directional guiding in the self-assembly process, others are significantly less directional (hydrophobic interactions and $\pi-\pi$ stacking). The directionality is especially important for creating one-dimensional molecular nanofibers (supramolecular polymers), and a variety of noncovalent polymeric systems based on hydrogen bonds in organic solvents has been developed.[5−8] In contrast, owing to the lack of directionality of hydrophobic interactions,[9] rational design of supramolecular polymers in water is challenging.[5,9−17] Usually, supramolecular polymers in aqueous medium are built from aromatic amphiphiles, which hydrophobic/π-stacking interactions result in the formation of continuous aromatic stacks. An alternative polymerization motif, employing directed pairwise hydrophobic interactions comparable in directionality to the hydrogen bonds, has been limited to designs in which one hydrophobic face of a primary aromatic unit is protected by a DNA scaffold,[15] or by a cavitand.[12] A more general approach to pairwise directional hydrophobic/π-stacking motifs is needed to broaden the scope of design strategies targeting supramolecular polymers.

Systems based on pairwise aromatic interactions may also possess unique photofunction due to the discontinuity of the aromatic pairs. The continuous aromatic stacks normally show fast exciton hopping following excitation with light, whereas exciton confinement is rarely observed in such π-stacked systems.[18−20] In the case of the pairwise attachment of aromatic units (stacked dimers) with relatively weak coupling between the pairs, weakly coupled low energy excimer-like states will form;[21] these are expected to trap excitons,[22] which may lead to spatially localized emission. Such exciton localization, resulting in the emission from spatially defined segments of the extended organic structures, can be useful for creation of addressable supramolecular luminescence devices.[18]

Here, we report on a rationally designed directional pairwise bonding motif that was used to assemble supramolecular polymers in aqueous medium. To the best of our knowledge, this is the first example of noncovalent polymers based on a directional pairwise hydrophobic motif using unprotected π-surfaces. Ultrafast laser studies revealed that the pairwise assembly mode enables exciton confinement, uncharacteristic of continuous stack systems. We believe that multivalent systems with adequately positioned aromatic moieties can be generally employed to impose directional pairwise bonding, enabling rational design of supramolecular
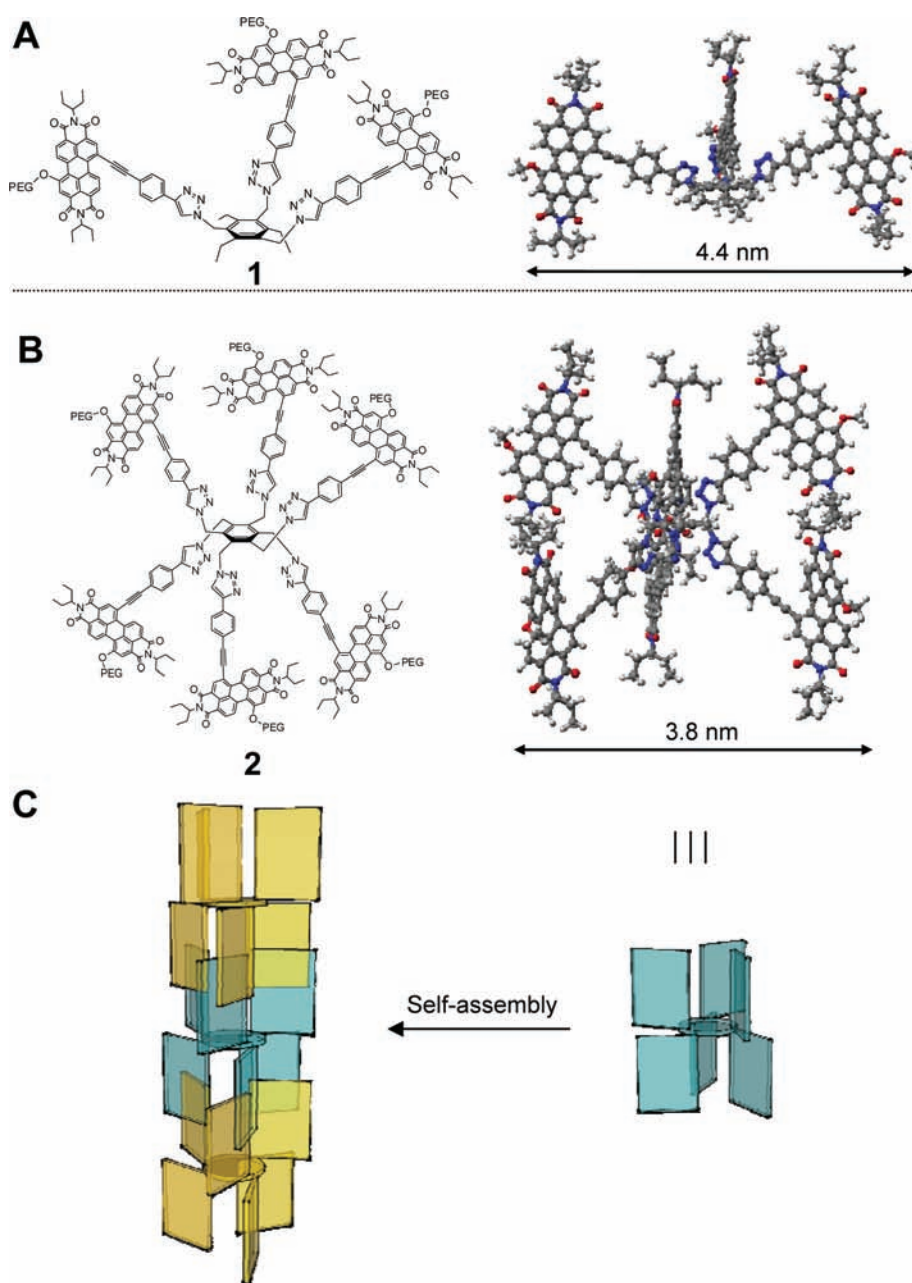
Figure 1. (A and B) Structure (left) and molecular models (right, optimized using molecular mechanics; hydrogens and PEG groups are omitted for clarity) of (A) **1** (PEG=$CH_2-CH_2(O-CH_2-CH_2)_{13}-CH_3$); (B) **2** (PEG=$CH_2-CH_2(O-CH_2-CH_2)_{16}-CH_3$). C) Illustration of the assembly pattern for compound **2**. For clarity, alternate molecular units have different colors.

polymers, with properties different from those of their continuous stack counterparts.

RESULTS AND DISCUSSION

Design. Our design of pairwise stacking/hydrophobic interactions was based on the idea that a rigid scaffold may restrict interactions between hydrophobic moieties, provided their hydrophobic surfaces are approximately *parallel to the axis of the scaffold* (and the polymer), contrasting to a conventional perpendicular arrangement (as in discotic systems). As a scaffold we employed hexa-substituted benzenes (HSB), bifacially segregated systems, whose 1,3,5 substituents are situated above the

phenyl plane and 2,4,6 ones below it, rendering HSB platforms advantageous for construction of tripodal ligands, receptors, and cages.[23,24] To create directional self-assembling motif based on $\pi-\pi$ stacking and hydrophobic interactions, we designed and synthesized (using click chemistry) **1** and **2**, in which aromatic amphiphiles (perylene diimide units (PDIs) bearing polyethylene glycol (PEG) substituents[14,25−30]) are attached to HSB scaffold through rigid linkers (Figure 1). Our modeling studies revealed sterically favorable alternate arrangement ("1,3,5 up/2, 4,6 down") of substituents in **1** and **2**, with the PDI cores approximately parallel to the scaffold axis (especially in sterically crowded **2**, Figure 1). The interaction between multiple PDI units (multivalent supramolecular interactions[31,32]) should further enhance the

directionality and bond strength, leading to one-dimensional assembly motif (Figure 1C).

Self-Assembly Studies. Compound **1** is largely disaggregated in chloroform and aggregated in most other organic solvents (Figure S5), whereas **2** shows substantial PDI stacking in all solvents, as indicated by UV—vis spectra (Figure S9). In water/THF mixtures, UV—vis of **1** and **2** show very similar broadened peaks with inverted intensity of 0—0 and 0—1 vibronic bands (Figure 2), a pattern typical for cofacial aggregation of PDI.[33] The fluorescence spectra of **1** and **2** are also very similar, showing broadened peaks with large Stokes shifts (Figure 2), characteristic of PDI excimer-like emission that is often observed for cofacial PDI stacks.[21,34]

Further insight into solution-phase self-assembly was obtained using cryogenic transmission electron microscopy (cryo-TEM).[35,36] It reveals that in a water/THF mixture (7:3 v/v) compound **1** assembles into fiber-like structures (Figures 3 and S10). The different contrast of the periphery and center of these structures is characteristic of the projection images of tubular aggregates (hollow cylinders),[29,37] and their high-contrast circular termini (end-caps) are also clearly observed (Figure 3). The

external diameter of the assemblies is 4.4 ± 0.3 nm, corresponding well to the diameter of the hydrophobic core of **1** (Figure 1). The diameter of the interior lower-contrast part is 2.6 ± 0.2 nm, and the high-contrast wall thickness is 0.9 ± 0.2 nm (see below for molecular modeling). The high-contrast structures are due to a hydrophobic core of the assembly as the contrast of solvated PEG groups is similar to the vitrified ice background.[35] The average length of the fibers is 166 ± 81 nm. Dynamic light scattering (DLS) of a water/THF solution (7:3 v/v) of **1** shows formation of relatively polydisperse aggregates with an average hydrodynamic radius of 219 ± 39 nm (Figure S34). Tube-like structures were also observed in solutions of **1** in neat water (Figure 4), obtained by evaporation of THF from water/THF (7:3 v/v) solution of **1**; they have a diameter of 4.3 ± 0.3 nm, and lengths of 188 ± 79 nm.

Similarly to **1**, compound **2** self-assembles into fibers in a water/THF mixture (7:3 v/v), as evidenced by cryo-TEM
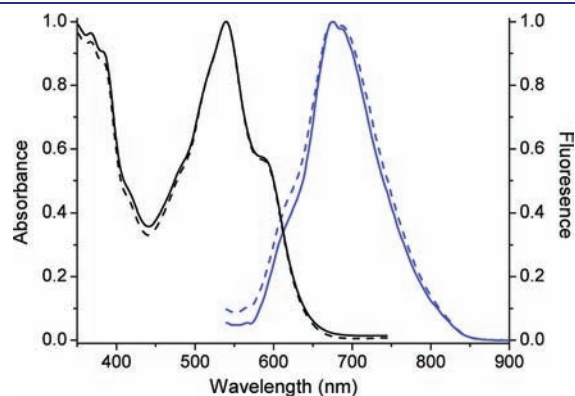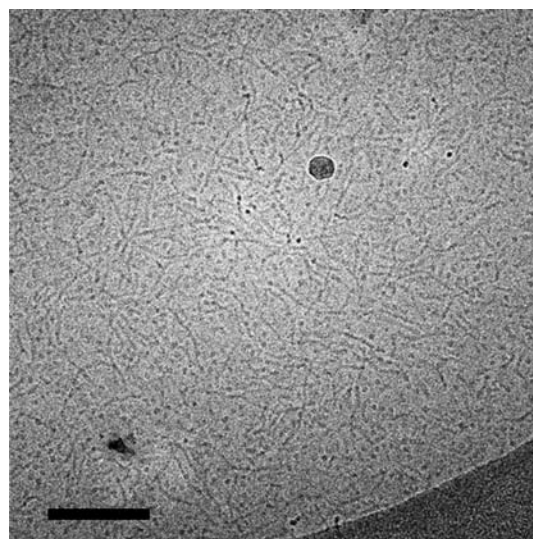

Figure 2. UV/vis (black traces) and fluorescence (blue traces) spectra (normalized) of **1** (solid line) and **2** (dashed line) in water/THF (70:30, v/v).

Figure 4. Cryo-TEM image of a solution of **1** (10^{-5} M) in water (scale bar: 200 nm).

Figure 3. Cryo-TEM images of a solution of **1** (1×10^{-5} M) in water/THF (7:3 v/v). (Left) Representative image of the vitrified solution; scale bar: 100 nm. (Right) High magnification images (scale bars: 20 nm).
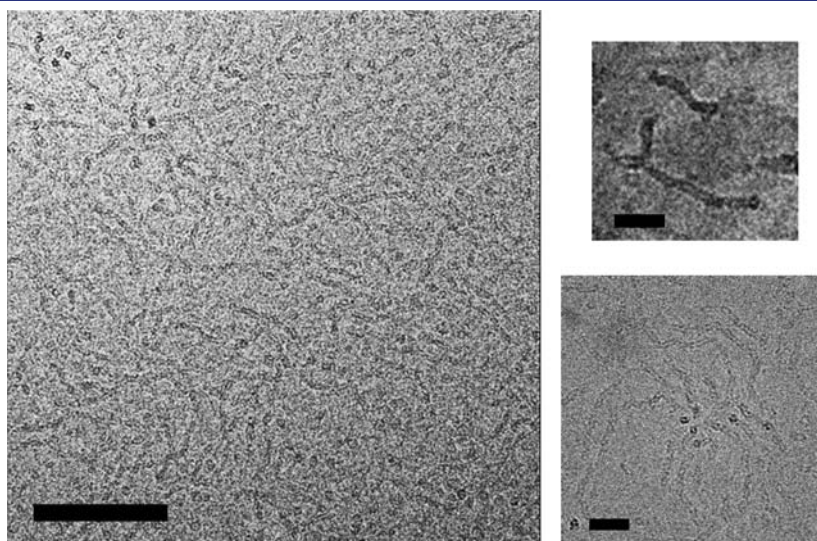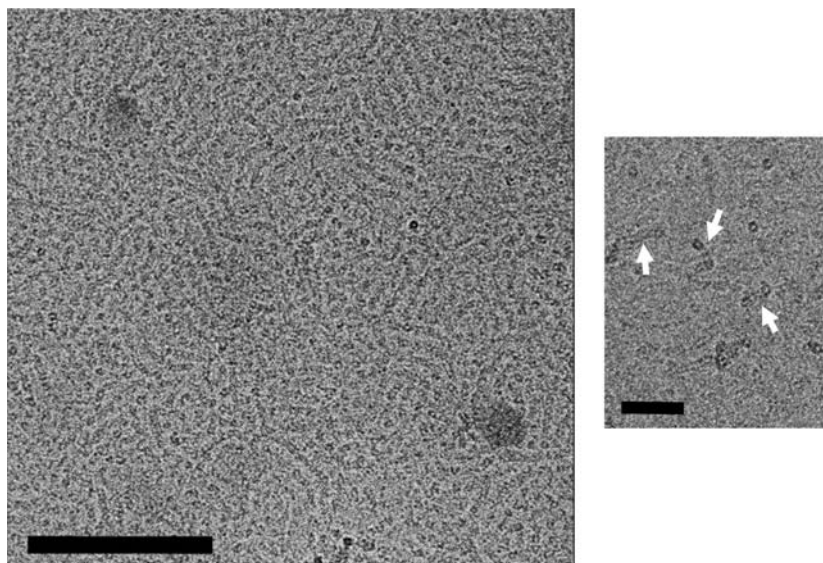
Figure 5. Cryo-TEM images of a solution of **2** (1×10^{-5} M) in water/THF (7:3 v/v). (Left) Representative image of the vitrified solution; scale bar: 100 nm. (Right) High magnification images; white arrows point at tubular aggregates (scale bar: 20 nm).
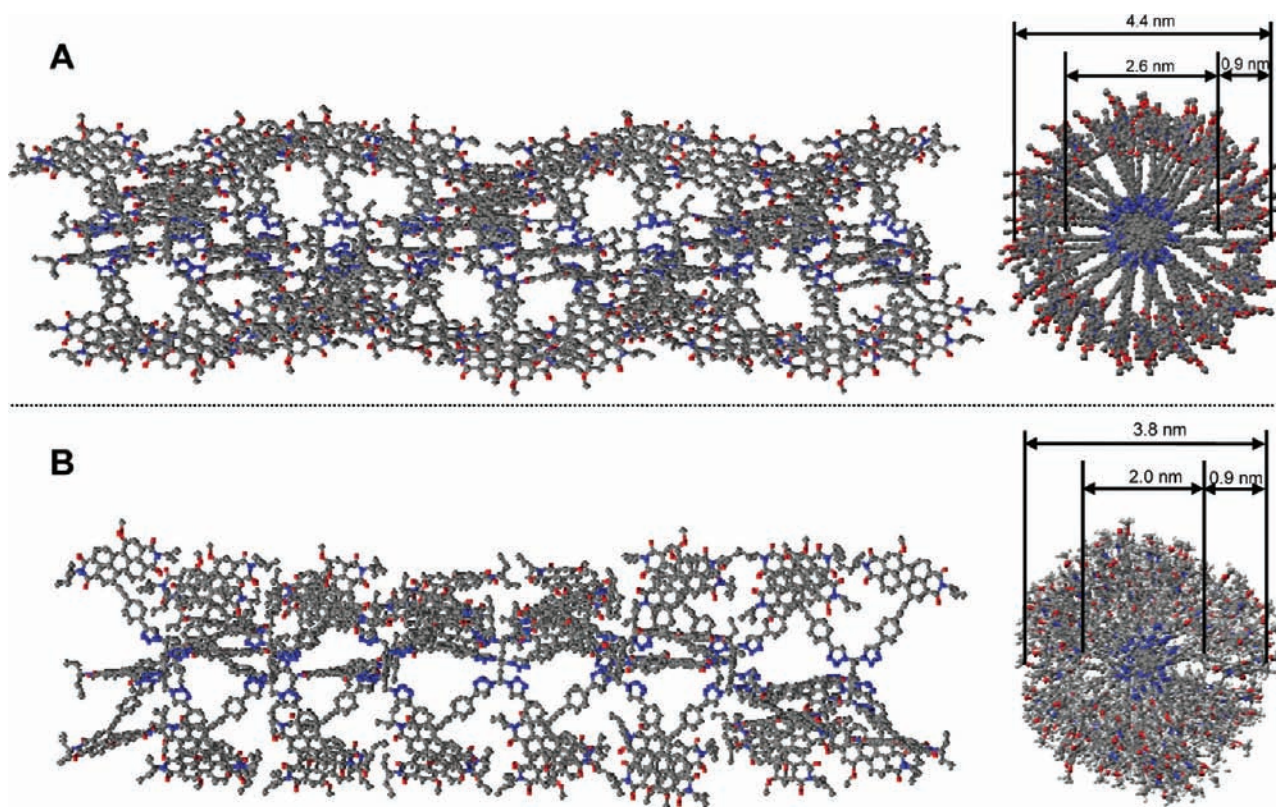

Figure 6. Molecular models (molecular mechanics optimization, MM2 and MM3 augmented force field). (Left) Side view; (right) top view. (A) Assembly based on **1** (22 molecules); (B) assembly based on **2** (7 molecules). Hydrogen atoms and PEG chains (located at the periphery of the tube) were omitted for clarity. Models of the assembly subunits are given in Figures S20–s25. For the enlarged versions of the models, see Figures S22 and S26.

(Figures 5 and S11). The fibers show tubular structures with a diameter of 3.8 ± 0.4 nm. The diameter of the interior lower-contrast part is 2.0 ± 0.2 nm, and the higher-contrast wall thickness is 0.9 ± 0.2 nm. The length of the nanotubes is 183 ± 96 nm. DLS showed formation of relatively polydisperse aggregates with an average hydrodynamic radius of 162 ± 62 nm (Figure S35). The fibrous structures assembled from **2** (3.8 ± 0.4 nm in diameter, having 237 ± 51 nm length) were observed also in pure water (Figure S12); however, amorphous darker-contrast arrays were present as well, most probably due to fiber fusion.
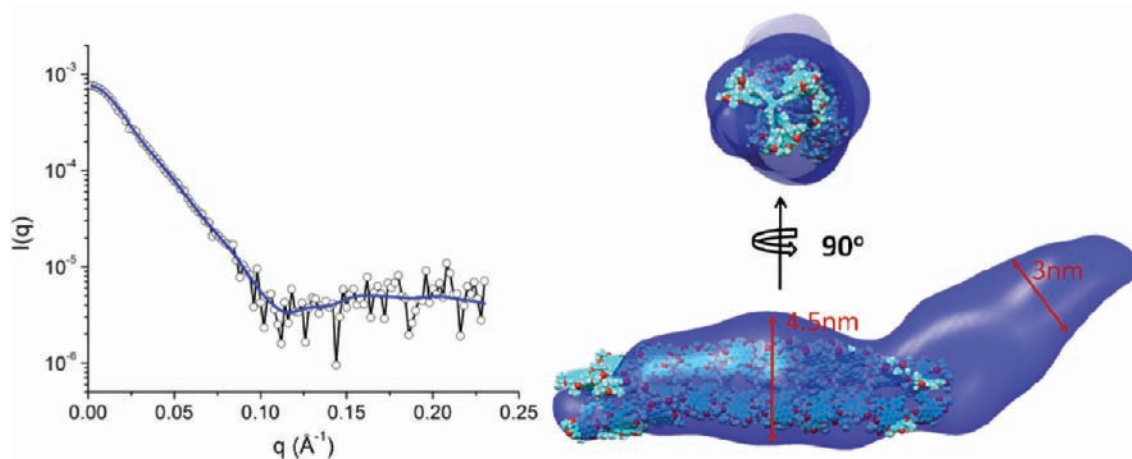
Figure 7. (Left) The SAXS profile of solution-phase sample **2** at 1×10^{-5} M in water/THF (70:30, v/v) and a representative envelope DAMMIN fit (blue solid line). (Right) The two views of the overlay of the SAXS molecular envelope (blue, in transparent surface mode) for **2** and the molecular model presented in Figure 6B.

Molecular models that are best fit for the assemblies observed in cryo-TEM are presented in Figure 6 (see Supporting Information for details). We note that only models showing pairwise interactions fit the imaged structures and their properties adequately. The models indicate that in the case of **1** two tripod molecules engage into pairwise interactions through the PDI aromatic surfaces (Figures S19−S21). The paired units undergo further assembly, interacting via hydrophobic surface created by the HSB ethyls and ethyl propyl groups of PDI, eventually leading to fibers (Figure 6A). PEG groups (one on each PDI) are located at the periphery of the structure. The tube-like appearance of the assembly is due to the high contrast of the "walls" constructed from the PDI units, and the lower contrast of the interior, owing to the lower density and lower contrast of the linker and phenyl units. The model dimensions are in excellent agreement with the cryo-TEM images. In the case of **2**, all the molecules in the fibril structure interact through the aromatic surfaces of PDI units (Figure 6B) located at both sides of the benzene core, as schematically depicted in Figure 1C. The structural parameters of the model are almost identical to the fiber dimensions observed in the cryo-TEM images. The model suggests that self-assembly of **2** results in compartmentalized fibers with cavities of ∼1 nm³. Their ability to encapsulate hydrophobic molecules is currently under study in our group.

It has been reported that upon partial reduction PDI radical anions embedded in cofacial stacks give rise to an EPR signal, whose width depends on a number of stacked PDIs involved in electron hopping.[38] Assemblies of **1** and **2** in THF/water (3:7) reduced with 0.25 equiv of sodium dithionite exhibited EPR signals with a peak width of 3.01 G (Figure S32), consistent with electron hopping between two PDIs,[38] further corroborating the pairwise PDI stacking.

Small Angle X-ray Scattering Studies. To further confirm the results of cryo-TEM and theoretical modeling, small-angle X-ray scattering (SAXS) using a synchrotron source (see Experimental Section for details) was employed to characterize the solution-phase structures of **1** and **2**. The structural envelopes for **1** and **2** reconstructed from SAXS data[39,40] adopt a cylinder-like shape, as displayed in Figures 7 and S36. The cross-sectional diameter of the SAXS envelope of **2** is about 3.0−4.5 nm throughout the structure, slightly smaller than that of **1**, which is

ca. 5.0 nm. In both cases, the SAXS envelope cross sections match well those obtained from molecular models, and in the case of **2**, both the overall structure of the envelope and its diameter fit almost completely those of the molecular model. The length of SAXS envelope of **2** is about 25 nm, while it is about 15 nm for **1**, both shorter than fiber lengths observed in cryo-TEM. This arises from the fact that our SAXS setup recorded scatterings from pair-distances no more than 50 nm (limited by the lowest achievable q-value); consequently, the SAXS envelopes reflect the portion of the tube lengths, rather than their full length.

Supramolecular Polymerization Studies. The self-assembly of PDI-based systems can be followed by UV−vis and/or fluorescence spectroscopy. Usually, in UV−vis absorption spectra, the intensity ratio of the $0 \rightarrow 0$ to the $0 \rightarrow 1$ vibronic bands of PDI can be used in order to quantify the degree of aggregation. However, for **1** and **2** in water/THF (7:3, v/v), the $0 \rightarrow 0/0 \rightarrow 1$ intensity ratio remains the same (0.53) throughout a wide concentration range, indicating a high degree of aggregation.

In general, self-assembly studies on highly aggregated systems are challenging, for example, making difficult estimation of equilibrium constants for self-assembly of aromatic systems in aqueous medium.[10] However, fluorescence of **1** and **2** allowed insight into their self-assembly. Thus, emission of **1** and **2** in water/THF solution gives rise to two components. The band (shoulder) at ∼620 nm arises from the residual fluorescence of the nonstacked PDI (similar to the emission spectra in chloroform), see Figures 2 and 8. The broad band at 700 nm is characteristic of excimer emission from the stacked PDI units.[21,34] This assignment is confirmed by our fluorescence lifetime studies: the shorter fluorescence lifetime at 620 nm (3.8 ns) is characteristic of nonstacked PDI, while the longer lifetime (10 ns) at 700 nm is typical of PDI excimer emission.[21] This is further corroborated by the concentration dependence studies. Lowering the concentration brings about growing in of the 620-nm peak (more pronounced in the case of **2**), indicating disaggregation (Figures S27 and S28). Higher sensitivity of emission spectra to disaggregation is due to a higher emission quantum yield of disaggregated PDI (∼20% for disaggregated **1** and **2**) in comparison to PDI excimer emission (0.5%, see Supporting Information). Thus, fluorescence spectra allowed estimating the
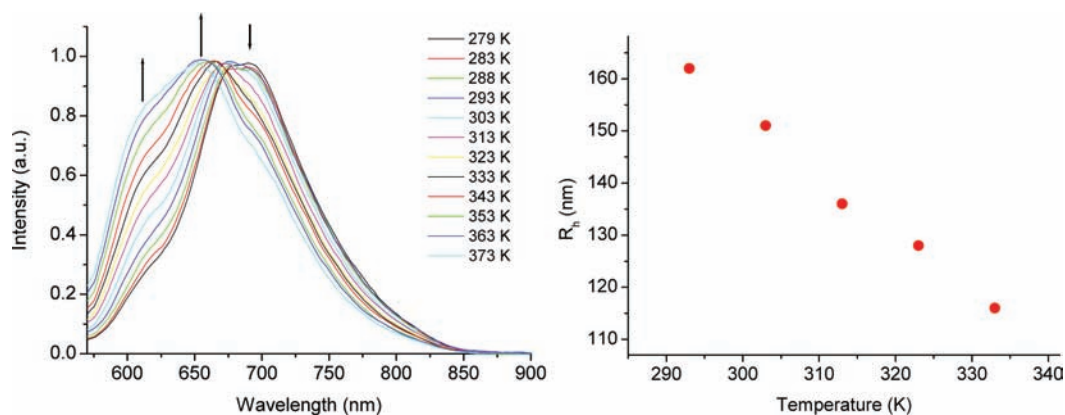
Figure 8. (Left) Normalized fluorescence of **2** (excitation at 520 nm), in THF/water (7:3, v/v), 10^{-5} M, temperature range 279−373K. Showing gradual depolymerization of the supramolecular polymer, as indicated by growing in of a peak at λ_{max} = 620 nm. Arrows indicates the change with increasing temperature. (Right) T-dependent DLS measurements of **2** in water/THF (7:3), $c = 10^{-5}$ M, showing gradual depolymerization (decrease in hydrodynamic radius R_h) as a function of rising temperature.
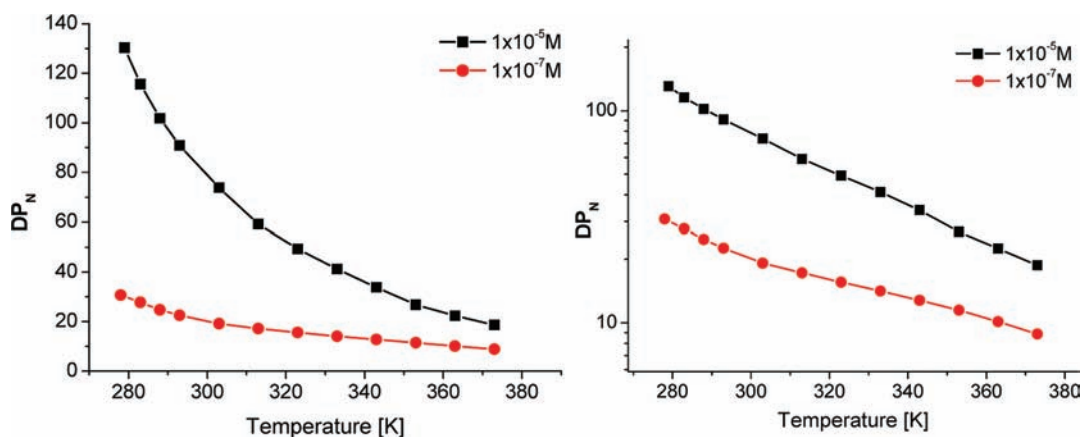

Figure 9. Average degree of polymerization (DP_N) for **2** in water/THF (7:3) at 1×10^{-5} M (black) and at 1×10^{-7} M (red) using linear (left) and logarithmic (right) scales.

ratio of aggregated versus disaggregated PDI, which was utilized to obtain polymerization parameters.

Supramolecular polymerization can be studied using concentration- or temperature-dependent (T-dependent) measurements. It was found that T-dependent measurements are especially useful for supramolecular polymerization studies and determination of thermodynamic parameters.[41,42] Since our concentration-dependent studies did not allow access to the regime where substantial depolymerization occurs (see Supporting Information for details), temperature-dependent studies were employed to obtain insight into supramolecular polymerization. Aggregates of **1** showed some degree of disassembly upon heating in water/THF solvent as indicated by UV−vis and fluorescence spectra; however, complex pattern of fluorescence spectra (most probably due to the formation of slightly different excimer states) did not allow reliable deconvolution of monomer and excimer fluorescence; this combined with insufficient changes in UV−vis spectra precludes assessment of self-assembly processes.

In the case of more rigid **2**, fluorescence spectra allowed reliable deconvolution. The T-dependent studies of **2** in water/THF (7:3) were performed at two concentrations: 1×10^{-5} M (used for cryo-TEM studies) and 1×10^{-7} M. To follow the

self-assembly of **2**, we recorded the fluorescence spectra at 10 K intervals while slowly heating the sample from 279 to 373 K at a rate of 1 K/min (Figure 8). This low heating rate was applied to ensure that the supramolecular polymerization occurred under equilibrium conditions. We also verified that upon cooling the fluorescence spectra are identical to the initial state. Deconvolution of monomer and excimer fluorescence was used to estimate the average degree of polymerization at each temperature (see Supporting Information for details). T-dependent DLS spectra of **2** confirmed gradual disassembly upon heating (Figure 8). T-dependent UV−vis spectra of **2** in water/THF (7:3) corroborate disaggregation at higher temperatures (Figure S31); however, they cannot be used for quantitative analysis. Degree of polymerization was estimated using a ratio between the deconvoluted fluorescence peaks that can be attributed to the aggregated and disaggregated PDI (see Supporting Information), analogously to the widely employed methodology that is based on distinct UV−vis features that are ascribed to aggregated and disaggregated species.[10,41]

The graph presented in Figure 9 shows temperature dependence of the degree of polymerization (DP_N), revealing gradual depolymerization as a function of increasing temperature: at 10^{-5} M from ∼130 units (at 279 K) to 19 units at 373 K, and at
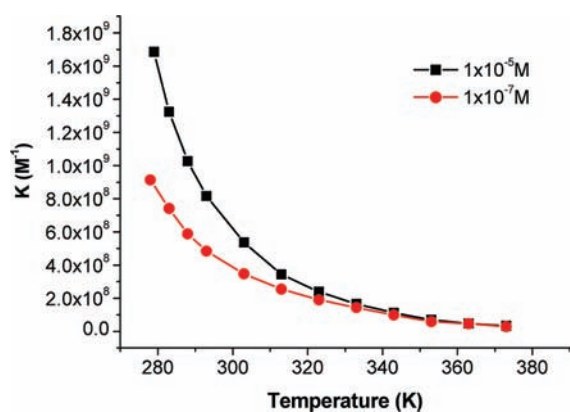
Figure 10. Elongation equilibrium constant, K, as a function of temperature. Calculated for compound **2** in water/THF (7:3, v/v) solution using eq 1.

Figure 11. Van't Hoff plot for **2** in water/THF (7:3, v/v), at 10^{-5} M, temperature range 279−373 K ($R^2 = 0.998$).

10^{-7} M from ∼32 units to 9 units. Under the experimental conditions, even at the lowest concentrations allowing reliable data analysis (10^{-7} M), we did not observe a fully disaggregated state; therefore, the determination of the supramolecular polymerization mechanism based on α (normalized degree of polymerization)[10,41] is unfeasible. Nevertheless, the average degree of polymerization (DP_N) can be used in order to identify the supramolecular polymerization mechanism. Thus, the linearity of temperature-dependent DP_N on a logarithmic scale is characteristic of isodesmic behavior.[42] Such behavior is expected for **2**, characterized by the identical interaction motif (3 stacked pairs of PDIs) along the polymer chain.

At room temperature and 10^{-5} M concentration of **2**, DP_N = 91. We can use this value to calculate the polymer chain length by multiplying this number by the monomer length. From molecular models, the benzene to benzene distance in the fiber based on **2** is 1.63 nm, giving the average chain length of 148 nm. These results are in agreement with the average chain lengths derived from the concentration dependent studies[5,10,43] (∼121 nm, Figure S30), and the polymer lengths observed in cryo-TEM images (183 ± 96 nm). Thus, our results are internally consistent.

We applied eq 1 in order to calculate equilibrium constants (K) of polymerization,[41] where c_T corresponds to the total concentration of **2** (Figure 10). The average equilibrium constant $K(293) = 8.2 \times 10^8$ M^{-1} is higher than the values of $(3.2-8.0) \times 10^7$ M^{-1} observed for self-assembly of PDI-capped DNA oligomers in aqueous media driven by pairwise interactions between PDIs.[15] We ascribe this to stronger multivalent interactions in the case of **2**. Using eqs 1 and 2, one can calculate the polydispersity index (PD) at equilibrium (c_T is the total concentration of monomer).[5,44]

$$DP_N = \frac{1}{2} + \frac{1}{2}\sqrt{4K(T)c_T + 1} \tag{1}$$

$$PD = 2 + \frac{1}{2Kc_T} - \left(\frac{1}{Kc_T} + \frac{1}{4(Kc_T)^2}\right)^{1/2} \tag{2}$$

At 293 K and $c_T = 10^{-5}$ M, $K = 8.2 \times 10^8$ and PD = 1.99. Such polydispersity index is typical for isodesmic polymers.[5] Plotting the logarithm of K versus the reciprocal temperature (van't Hoff plot, Figure 11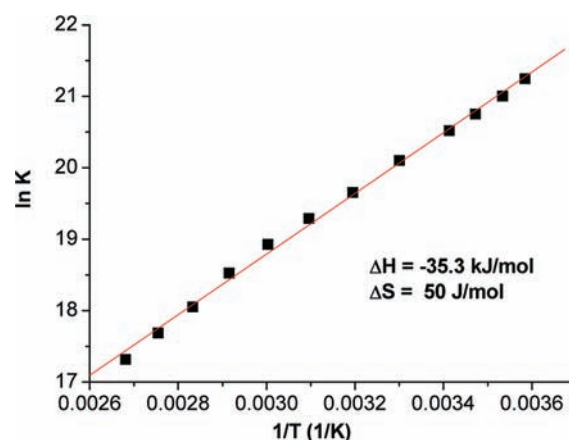), affords the thermodynamic parameters of supramolecular polymerization: $\Delta H = -35.3$ kJ/mol and $\Delta S = 50.0$ J/mol; ΔG (293) $= \Delta H - T\Delta S = -50.2$ kJ/mol.

Importantly, the supramolecular polymerization of **2** appears to be both enthalpically and entropically driven. Enthalpy-driven hydrophobic interactions are not common,[45] yet they should be dominant in the case of large hydrophobic surfaces such as in **2**.[46] Enthalpy-driven supramolecular polymerization in water ($\Delta H = -40$ kJ/mol) that involves fluorinated discotic amphiphiles has been recently reported.[13]

Photonic Studies. To investigate the exciton dynamics in the supramolecular polymers, we performed time-resolved photophysical studies on the assemblies of **1** and **2** (see Supporting Information for details). Both systems show very similar behavior. Femtosecond transient absorption spectra following excitation with a 400-nm laser pulse reveal formation of ^{1*}PDI peak in both assemblies within the instrument response time (300 fs, Figures S13 and S17). Global fit analysis (Figure 12) reveals species-associated difference spectra (SADS) that show formation of short-lived ^{1*}PDI state (2.8 ps, black trace) and two states exhibiting red-shifted peaks with longer decay times. Kinetic traces corroborate global fit analysis showing 2 ps rise times, corresponding to the red-shifted peaks (Figure 12). Such behavior is typical of ultrafast dynamics of excimer formation in stacked PDI dimers, characterized by appearance of red-shifted excimer features in 1−2 ps.[21] This is further supported by the appearance of broad red-shifted fluorescence peaks (Figure 2), with long lifetimes (∼10 ns as revealed by fluorescence lifetime studies) typical of PDI excimers.[21,34] Remarkably, unlike in the case of extended PDI stacks,[29,34] almost no dependence of the kinetics on the laser power was observed (Figure 12, Tables S1, S2), indicating that exciton annihilation that results from exciton hopping did not occur. Thus, excitons are confined in the fibers assembled from **1** and **2**, in striking contrast to efficient exciton movement in supramolecular systems based on extended π-stacks.[29,30,34,47,48] Exciton trapping due to excimer formation[22] should be general for the pairwise stacking morphology, rendering pairwise motif useful for exciton confinement. The latter can bring about emission from spatially defined segments of the assemblies (excimer emission in the self-assembled **1** and **2**), which is uncommon for extended aromatic structures. It was suggested that such unique photonics may be employed in supramolecular luminescence devices.[18] Confined excitons have been recently
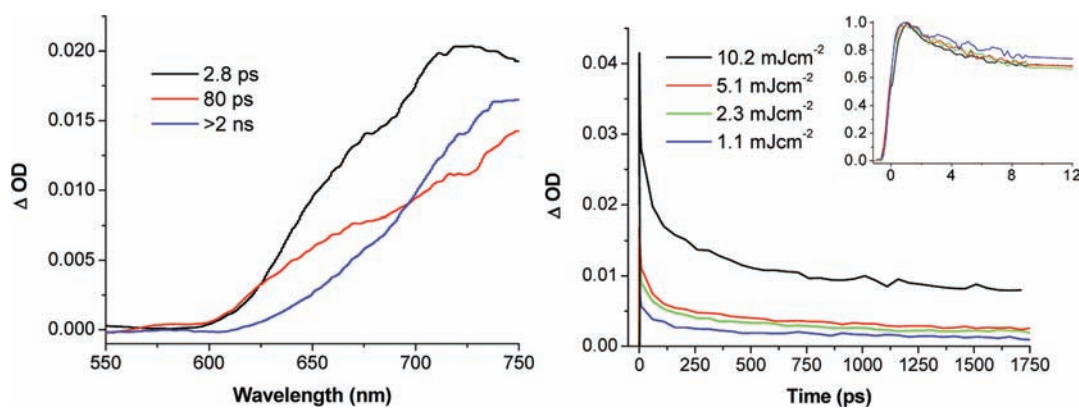
Figure 12. Transient absorption of **2** in water/THF (70:30, v/v). (Left) Species-associated difference spectra (SADS) obtained by global fit analysis. (Right) Decay kinetics following excitation with different pump fluences and probed at the absorption peak (740 nm). The inset shows the first 12 ps of the normalized transients, which exhibit almost no power dependence. Both SADS and kinetics indicate formation of a red-shifted excited state peak in ~2 ps, typical of excimer formation.

observed in several aromatic peptide assemblies[18,19] and in DNA.[20]

In conclusion, supramolecular polymerization in aqueous medium based on directional pairwise hydrophopic interactions was demonstrated. We show that directional hydrophobic interactions leading to supramolecular polymerization can be rationally designed, employing noncovalent multivalency and rigid geometry with aromatic units positioned parallel to the polymer axis. Supramolecular polymerization of **2** was studied, revealing strong association constants (10^9 M^{-1}). Thermodynamic parameters of the process indicate that it is both enthalpically and entropically driven, with the dominant enthalpic contribution that arises due to the large hydrophobic surfaces involved in polymer formation. The photonic properties of the supramolecular polymers based on aromatic pairwise interactions differ significantly from the continuous stack systems, enabling exciton confinement that leads to localized emission. Directional pairwise hydrophobic interactions regulated by scaffold geometry introduce a new strategy for rational design in aqueous noncovalent synthesis, and result in arrays with functions unattainable in conventional π-stacked systems.

■ EXPERIMENTAL SECTION

All procedures with air and moisture-sensitive compounds were performed in a glovebox (MBraun, LABmaster) under a dry nitrogen atmosphere or on a high vacuum line using Schlenk techniques. Unless otherwise indicated, all starting materials were obtained from commercial suppliers and were used without further purification. Poly(ethyleneglycol) methyl ether (PEG) was purchased from Aldrich (molecular weight of approximately 750 g/mol, which corresponds to a chain length of about 17 monomer units). It was dried over molecular sieves (3 Å) for 3 days in a glovebox prior to use. Organic solvents were purchased in the purest form available, degassed by purging with argon and kept over molecular sieves (3 Å) in the glovebox. For all aqueous mixtures, double-distilled water was used (Barnstead NANOpure Diamond water system).

CAUTION! Hexakis(azidomethyl)benzene and 1,3,5-tris(azidomethyl)-2,4,6-triethylbenzene are stable at room temperature,[49] yet they should be handled with care on account of explosiveness of organic azides.[49] Sodium azide should be also handled with care due to its toxicity and possible explosiveness.

The samples of supramolecular structures were prepared by dissolving compound **1** and **2** in THF and subsequent addition of water into the

mixture until the desired THF/water volume ratio was achieved. Clear homogeneous solutions were obtained that were aged for 24 h. Longer aging does not result in significant change in samples appearance and morphologies as evidenced by cryo-TEM. To obtain solution in neat water, the water/THF solutions of **1** and **2** were prepared as described above, then THF was fully evaporated (as verified by NMR and NIR spectra) and water was added to bring the samples to the desired concentrations.

The ^{1}H, ^{13}C spectra were recorded at 20 °C on 400 MHz NMR spectrometer (Bruker). ^{1}H, ^{13}C{^{1}H} chemical shifts are reported in parts per million (ppm) downfield from tetramethylsilane (δ scale). ^{1}H NMR chemical shifts were referenced to the residual hydrogen signal of CDCl$_3$ (7.26 ppm). In ^{13}C{^{1}H} NMR measurements, the signal of CDCl$_3$ (77.16 ppm) was used as a reference. Coupling constants (J) are reported in hertz (Hz), and splitting patterns are designated as s (singlet), d (doublet), t (triplet), q (quartet), m (multiplet), b (broad).

MALDI-TOF mass-spectrometry measurements were performed using REFLEX reflector time-of-flight instrument with SCOUT multiprobe (384) inlet.

Analytical gel permeation chromatography (GPC) was preformed using a Varian PrepStar 218 HPLC pump, Varian ProStar model 325 UV−vis detector, and a Varian/Polymer Laboratories PLgel Olexis 7.5 × 300 mm column with THF as an eluent. The temperature was set at 40 °C. The system was calibrated using polystyrene standards.

Dynamic light scattering measurements were performed on a Viscotek 802 DLS instrument with detection at right angle using a laser wavelength of 830 nm. The data were analyzed by Omnisize 2.0 software with a correlator resolution 256 channel.

UV−vis absorption measurements were carried out on a Cary-5000 spectrometer (Varian). Steady-state fluorescence measurements were performed on a Cary Eclipse fluorimeter (Varian) with excitation/emission geometry at right angles. Fluorescence quantum yields were determined using standard procedure.[50] *Sulforodamine* 101 solution in ethanol (λ_{abs} = 576 nm, λ_{em} = 592 nm, φ = 0.9) was used as a fluorescence reference. Quantum yield measurements were made using three excitation wavelengths: 480, 500, 520 nm. The quantum yields were averaged over 30 measurements.

To study supramolecular polymerization, we recorded the fluorescence spectra slowly heating the sample from 279 to 373 K at a rate of 1 K/min. All the measurements were performed in tightly sealed screwcup cuvettes equipped with Teflon linear for better sealing. The head space volume in the cuvettes was completely filled with the sample solutions. Reproducibility of the fluorescence data was verified in several independent measurements that showed identical spectra and unchanged sample volume. The equilibrium constants and thermodynamic

values in the 279—343 K temperature range are almost identical to those obtained using the 279—373 K temperature range.

Fluorescence lifetime measurements were performed by the time correlated single photon counting technique using FluoroCube (HORIBA Jobin Yvon) station equipped with TBX-04 detection module of less than 180 ps typical timing jitter and less than 100 ps overall time resolution. The instrument response function was obtained by measuring scattering from a standard sample (Ludox) with the monochromator set for detection at or close to the excitation source wavelength and remaining all other parameters unchanged. Samples were excited using a laser diode (NanoLED 406 L) that generated 200 ps pulses of 406 nm light. The samples were excited with 1 MHz repetition rate and 10 000 counts in the peak channel were collected. Lifetime decays were deconvoluted and fitted using Das6 decay analysis software.

Electrochemical measurements were performed using a CH Instruments electrochemical workstation, model 660C. Methylene chloride containing 0.1 M tetra-n-butylammonium hexafluorophosphate (TBAPF$_6$) electrolyte was used as a solvent. A platinum disk electrode (2.0 mm diameter) was employed as a working electrode, and platinum wires as counter and auxiliary electrodes. Ferrocene/ferrocenium (Fc/Fc+: 0.475 V in CH$_2$Cl$_2$) was used as an internal reference for all measurements. All electrochemical measurements were performed in a nitrogen filled glovebox.

EPR spectra were acquired with a Bruker E-580 spectrometer, fitted with an EN801 resonator. Temperatures were maintained at 290 K. Samples of **1** and **2** (10−5 M in deoxygenated water/THF solution) that reacted with 0.25 equiv sodium dithionite were loaded in 2 mm quartz tubes in a nitrogen filled glovebox and sealed with grease and parafilm before the EPR measurements.

Computations were carried out using Scigress Explorer Ultra (7.7.0.49). Geometry optimization of **1** and **2** were performed in vacuum using molecular mechanics (MM2 and MM3 force field) and semiempirical PM6-D2MOZYME method as implemented in MO-PAC2009. Molecular dynamics (MD) simulations were performed in vacuum at 300 K, using the augmented Allinger's MM3 force field (aug-MM3), as implemented in Scigress Explorer. Different initial conformations were considered varying the relative orientation of the PDI units. For simplification, the PEG tail of the model was only 1 monomer unit long.

Cryo-transmission electron microscopy was performed using a Tecnai F20 transmission electron microscope operating at 200 kV, and using a Gatan 626 cooling holder and transfer station with a Gatan US4000 CCD digital camera, or a Tecnai T12 transmission electron microscope operated at 120 kV, using a Gatan 626 cooling holder and transfer station, with a TVIPS F244HD CCD digital camera. For sample-preparation, 8 μL of the sample was applied to a 300-mesh copper grid coated with holey carbon (Pacific Grid-Tech supplies). Samples were blotted at 25 °C and 100% relative humidity, and subsequently plunged into liquid ethane using Leica EM-GP Automatic Grid Plunger. Specimens were equilibrated at −178 °C in the microscope prior to imaging. The images were analyzed using AnalySIS 5.0 (2004, Soft Imaging System GmbH). The pictures were taken with a defocus value optimized for the specific magnification (e.g., we used −1.1 ± 0.4 μm defocus for 59K magnification). For consistency and accuracy, the widths of the fibers were measured using images taken at 59K magnification. The width measurements include the arithmetic mean and standard deviation of at least 50 structures.

Small-angle X-ray scattering (SAXS) was performed at beamline 12-ID of Advanced Photon Sources (APS) at Argonne National Laboratory (Chicago site). The wavelength, λ, of X-ray radiation was set as 0.689 Å. An X-ray flow cell made of a cylindrical quartz capillary with a diameter of 1.5 mm and a wall of 10 μm was used. The X-ray beam with size of 0.1 × 0.2 mm^2 was adjusted to pass through the center of the cell. The

exposure time was set to 1.0 s to avoid detector saturation and radiation damage. Potential radiation damage was further reduced by flowing the samples. The range of momentum transfer q [$= 4\pi \sin \theta/\lambda$, where 2θ is the scattering angle] of SAXS experiments was 0.006−0.23 Å^{-1}, with the capability of characterizing objects with length up to 50 nm. The samples were run at a concentration 1×10^{-5} M. To obtain good statistics, 150 images were taken for each sample and the background solvent. The 2-D scattering images of the solvents and samples were azimuthally averaged after solid angle correction and then normalized with the intensity of the transmitted X-ray beam. The resulting 1-D scattering data sets were averaged before solvent background subtraction. The scattering signal from the samples were obtained through subtraction of buffer scattering from sample scattering, then smoothed using OriginPro 8.5 (http://www.originlab.com/) with 5-points Savitz-ky-Golay method to further reduce noise level. The scattering intensities at and near $q = 0$ were extrapolated with the Guinier equation (eq 3):

$$I(q) = I_o \exp(- R_g^2 q^2/3) \tag{3}$$

where R_g is the radius of gyration and I_o is the forward scattering, the scattering intensity at $q = 0$. Both R_g and I_o were calculated from data at low q-values in the range of $qR_g < 1.0$ and used in the extrapolation to $q = 0$.

The program DAMMIN[39] was used to calculate an approximate molecular envelope. Scattering data in q range of 0−0.23 Å^{-1} were using in the calculation, and 24 calculations were performed for each sample in the "slow" mode. The resulting structural models were subjected to averaging using the program package DAMAVER[51] to obtain the most probable model. The averaged normalized spatial discrepancy (NSD) values between each pair of models were 1.0 for **1** and 0.8 for **2**, indicating good convergence among individual calculated structural models. Program Situs[52] was used to generate the final smooth SAXS structural envelopes from the averaged DAMMIN model.

Femtosecond transient absorption spectroscopy was performed using a system seeded by a modelocked Ti:sapphire oscillator (Spectra Physics Tsunami) pumped by a CW diode pumped Nd:YVO4 laser (Millennia Pro X). The oscillator produces a train of <100-fs pulses (bandwidth ∼10 nm fwhm), with a peak wavelength at around 785 nm, typically of 850 mW, corresponding to ∼10 nJ per pulse. The weak oscillator pulses are amplified by a chirped pulse regenerative amplifier (CPA) (Spectra Physics Spitfire). The pulses are first stretched, then regeneratively amplified in a Ti:sapphire cavity, pumped by a pulsed Nd:YLF laser (Spectra Physics Evolution-15) operating at 1 kHz. After the pulse has been amplified and recompressed, its energy is about 1.0 mJ in a train of 500 Hz pulses. An independent pump pulse is obtained by pumping an optical parametric amplifier (Spectra Physics OPA-800CF) that produces 120-fs pulses tunable from 300 nm to 3 μm.

The output power of the OPA is a few microjoules (depending on the chosen wavelength) at 500 Hz. The pump beam is mechanically chopped at half the amplifier repetition rate. The chopper (C-995 TTI) is synchronized with the Spitfire pulses. Normally, 2000 pulse pairs (pump on/pump off) are averaged to produce a transient absorption spectrum with a noise level below 0.3 mOD.

A small portion of the remaining amplified pulse is used to generate a white light continuum as a probe pulse. To this end, the Ti:sapphire beam is focused onto a 3-mm thick sapphire disk by a 10-cm focal length lens, and the numerical aperture of the beam is controlled by an iris placed in front of the lens to obtain a stable and smooth white light continuum. The resulting beam is passed through a Raman Notch filter (Semrock, Inc.) to remove the remains of the fundamental beam from the probe white light continuum.

The pump and probe pulses are crossed in the sample at a small angle, while maintaining a magic angle between the pump and probe polarizations. The remains of the pump pulse are removed by an iris, and the probe light is focused into an optical fiber that brings it into an imaging

interface, which focuses the light onto the entrance slit of a Jobin Yvon Triax 180 spectrograph. The light is normally dispersed by a 300 gr/mm grating onto a fast CCD camera (Andor Newton DU-970N-UV, operating at 500 spectra per second using "crop mode"). The whole setup is controlled by National Instruments LabView software.

The pump power intensities were kept ∼180−200 uW at 250 Hz (chopper frequency) as measured using Ophir thermal head power-meter in proximity to the sample. The laser spot of 300 μm diameter on the sample was measured by placing beamprofiler (Ophir Beamstar FX33) at the sample position and determining the 4-sigma (95% of the power) parameter. In the reported experiments, the pump was turned to about 400 nm by doubling the fundamental beam using a BBO crystal, and the optical densities of the samples (in 4 mm optical path length cuvettes) were kept between 0.2 and 0.5 at the peak wavelength. Experiments using 540 nm pump revealed identical behavior.

The instrument response function (300 fs) was recorded by repetition of the experiments with sample replaced by pure solvent and keeping all other parameters unchanged. Spectral corrections and analysis were performed using Surface Xplorer Pro (Ultrafast Systems) and Origin 7.5 (OriginLab) software.

Compound 1. In a nitrogen filled glovebox, 1,7-PEG-PDI-1,4-diethynylbenzene[53] (55 mg, 0.042 mmol), 1,3,5-tris(azidomethyl)-2,4,6-triethylbenzene[54] (4.6 mg, 0.014 mmol), and CuI (66.5 mg, 0.35 mmol) were dissolved in 30 mL of THF in the pressure flask; then, an aqueous solution (3 mL) of sodium ascorbate (138.6 mg, 0.7 mmol) was added to the reaction mixture. After sealing the pressure flask, the reaction was stirred at 75 °C for 4 days, in the absence of light, followed by solvent removal under vacuum. The residue was dissolved in chloroform and subjected to silica gel chromatography using chloroform/methanol (95:5, v/v) mixture as an eluent to yield 15 mg (25%) of **1** as a dark-purple solid.

^{1}H NMR (CDCl$_3$): δ = 10.05 (d, 3H, J_{HH} = 8.4 Hz, PDI), 9.47 (d, 3H, J_{HH} = 8.4 Hz, PDI), 8.56 (s, 3H, PDI), 8.50 (d, 3H, J_{HH} = 8.4 Hz, PDI), 8.40 (d, 3H, J_{HH} = 8.4 Hz, ArH), 8.18 (s, 3H, PDI), 7.86 (d, 6H, J_{HH} = 8.1 Hz, ArH), 7.63 (d, 6H, J_{HH} = 8.1 Hz, ArH), 7.45 (s, 3H CH), 5.85 (s, 6H, CH$_2$), 4.98 (m, 6H, CH), 4.52 (bm, 6H, CH$_2$), 4.11 (bm, 6H, CH$_2$), 3.50−3.90 (m, 156H, CH$_2$), 3.37 (s, 9H, CH$_3$), 2.94 (q, 6H, J_{HH} = 7.5 Hz, CH$_2$), 2.24 (m, 12H, CH$_2$), 2.00 (m, 12H, CH$_2$), 1.19 (t, 9H, J_{HH} = 7.5 Hz, CH$_3$), 0.97 (t, 18H, J_{HH} = 7.5 Hz, CH$_3$), 0.96 (t, 18H, J_{HH} = 7.5 Hz, CH$_3$).

^{13}C{^{1}H} NMR (CDCl$_3$): 164.09, 156.97, 147.36, 146.77, 137.19, 134.12, 133.78, 133.27, 132.46, 131.17, 130.23, 128.88, 128.41, 127.77, 127.50, 126.12, 123.72, 120.31, 119.21, 118.44, 98.07, 92.57, 72.06, 71.11, 70.95, 70.82, 70.69 (m, unresolved signals of PEG), 69.53, 69.13, 59.19, 57.99, 57.83, 48.32, 25.14, 25.09, 23.89, 15.93, 11.67, 11.55. MS MALDI-TOF (m/z): [M + Na$^+$], calcd. for PEG-14, C$_{234}$H$_{297}$N$_{15}$NaO$_{57}$, 4254.91; found, 4255.70. PD = 1.24. UV−vis (CHCl$_3$): λ_{abs}/nm (ε/M^{-1} cm^{-1}) = 579 nm (43500), 540 nm (45100). Fluorescence (CHCl$_3$): λ_{max}/nm = 605 nm; Φ_f = 0.15. Electrochemistry: Redox potentials in DCM (V vs SCE), Ered$_1$ = −0.64; Ered$_2$ = −0.83; Eox$_1$ = 1.48.

NMR, UV−vis, GPC, and mass spectra of **1** are presented in the Supporting Information.

Compound 2. In a nitrogen filled glovebox, 1,7-PEG-PDI-1,4−diethynylbenzene[53] (42.5 mg, 0.029 mmol), hexakis(azidomethyl)-benzene[49] (2.0 mg, 0.005 mmol), and CuI (66.5 mg, 0.35 mmol) were dissolved in 30 mL of THF in the pressure flask; then, an aqueous solution (3 mL) of sodium ascorbate (138.6 mg, 0.7 mmol) was added to the reaction mixture. After sealing the pressure flask, the reaction was allowed to stir at 80 °C for 4 days, in the absence of light, followed by solvent removal under vacuum. The resulting solid was dissolved in chloroform and subjected to silica gel chromatography using chloroform/methanol (93:7, v/v) mixture as an eluent to yield 18 mg (30%) of **2** as a dark-purple solid.

NMR: extensive broadening in the aromatic and aliphatic regions precluded characterization of **2** using ^{1}H and ^{13}C NMR spectrometry. MS MALDI-TOF (m/z): [M + Na$^+$], calcd. for PEG-17, C$_{490}$H$_{644}$N$_{30}$NaO$_{134}$, 9115.4; found, 9115.5. PD = 1.4. UV−vis (CHCl$_3$): λ_{abs}/nm (ε/M^{-1} cm^{-1}) = 580 nm (113000), 541 nm (131400). Fluorescence (CHCl$_3$): λ_{max}/nm = 605 nm; Φ_f = 0.20. Electrochemistry: Redox potentials in DCM (V vs SCE), Ered$_1$ = −0.60; Ered$_2$ = −0.80; Eox$_1$ = 1.49.

UV−vis, GPC, and mass spectra of **2** are presented in the Supporting Information.

■ ASSOCIATED CONTENT

S **Supporting Information.** Experimental details of synthesis and characterization, optical and EPR spectra, additional electron microscopy images, SAXS data, and temperature dependent data. This material is available free of charge via the Internet at http://pubs.acs.org.

■ AUTHOR INFORMATION

Corresponding Author
boris.rybtchinski@weizmann.ac.il

■ ACKNOWLEDGMENT

■ REFERENCES

(1) Stupp, S. I.; LeBonheur, V.; Walker, K.; Li, L. S.; Huggins, K. E.; Keser, M.; Amstutz, A. Science 1997, 276, 384–389.

(2) Lehn, J.-M. Science 2002, 295, 2400–2403.

(3) Reinhoudt, D. N.; Crego-Calama, M. Science 2002, 295, 2403–2407.

(4) Stoddart, J. F. Nat. Chem. 2009, 1, 14–15.

(5) De Greef, T. F. A.; Smulders, M. M. J.; Wolffs, M.; Schenning, A. P. H. J.; Sijbesma, R. P.; Meijer, E. W. Chem. Rev. 2009, 109, 5687–5754.

(6) Brunsveld, L.; Folmer, B. J. B.; Meijer, E. W.; Sijbesma, R. P. Chem. Rev. 2001, 101, 4071–4097.

(7) Zimmerman, S. C.; Zeng, F.; Reichert, D. E. C.; Kolotuchin, S. V. Science 1996, 271, 1095–1098.

(8) Castellano, R. K.; Rudkevich, D. M.; Rebek, J. Proc. Natl. Acad. Sci. U.S.A. 1997, 94, 7132–7137.

(9) Rehm, T. H.; Schmuck, C. Chem. Soc. Rev. 2010, 39, 3597–3611.

(10) Chen, Z.; Lohr, A.; Saha-Moller, C. R.; Würthner, F. Chem. Soc. Rev. 2009, 38, 564–584.

(11) Harada, A. J. Polym. Sci., Part A: Polym. Chem. 2006, 44, 5113–5119.

(12) Zayed, J. M.; Nouvel, N.; Rauwald, U.; Scherman, O. A. Chem. Soc. Rev. 2010, 39, 2806–2816.

16210

dx.doi.org/10.1021/ja2066225 |J. Am. Chem. Soc. 2011, 133, 16201–16211

(13) Besenius, P.; Portale, G.; Bomans, P. H. H.; Janssen, H. M.; Palmans, A. R. A.; Meijer, E. W. *Proc. Natl. Acad. Sci. U.S.A.* **2010**, *107*, 17888–17893.

(14) Baram, J.; Shirman, E.; Ben-Shitrit, N.; Ustinov, A.; Weissman, H.; Pinkas, I.; Wolf, S. G.; Rybtchinski, B. *J. Am. Chem. Soc.* **2008**, *130*, 14966–14967.

(15) Neelakandan, P. P.; Pan, Z. Z.; Hariharan, M.; Zheng, Y.; Weissman, H.; Rybtchinski, B.; Lewis, F. D. *J. Am. Chem. Soc.* **2010**, *132*, 15808–15813.

(16) Arnaud, A.; Belleney, J.; Boue, F.; Bouteiller, L.; Carrot, G.; Wintgens, W. *Angew. Chem., Int. Ed.* **2004**, *43*, 1718–1721.

(17) Obert, E.; Bellot, M.; Bouteiller, L.; Andrioletti, F.; Lehen-Ferrenbach, C.; Boue, F. *J. Am. Chem. Soc.* **2007**, *129*, 15601–15605.

(18) Amdursky, N.; Gazit, E.; Rosenman, G. *Adv. Mater.* **2010**, *22*, 2311–2315.

(19) Amdursky, N.; Molotskii, M.; Gazit, E.; Rosenman, G. *Appl. Phys. Lett.* **2009**, *94*, No. 261907.

(20) Buchvarov, I.; Wang, Q.; Raytchev, M.; Trifonov, A.; Fiebig, T. *Proc. Natl. Acad. Sci. U.S.A.* **2007**, *104*, 4794–4797.

(21) Giaimo, J. M.; Lockard, J. V.; Sinks, L. E.; Scott, A. M.; Wilson, T. M.; Wasielewski, M. R. *J. Phys. Chem. A* **2008**, *112*, 2322–2330.

(22) Fink, R. F.; Seibt, J.; Engel, V.; Renz, M.; Kaupp, M.; Lochbrunner, S.; Zhao, H. M.; Pfister, J.; Würthner, F.; Engels, B. *J. Am. Chem. Soc.* **2008**, *130*, 12858–12859.

(23) Kilway, K. V.; Siegel, J. S. *Tetrahedron* **2001**, *57*, 3615–3627.

(24) Hennrich, G.; Anslyn, E. V. *Chem.—Eur. J.* **2002**, *8*, 2219–2224.

(25) Gebers, J.; Rolland, D.; Frauenrath, H. *Angew. Chem., Int. Ed.* **2009**, *48*, 4480–4483.

(26) Zhang, X.; Rehm, S.; Safont-Sempere, M. M.; Würthner, F. *Nat. Chem.* **2009**, *1*, 623–629.

(27) Zhang, X.; Chen, Z.; Würthner, F. *J. Am. Chem. Soc.* **2007**, *129*, 4886–4887.

(28) Ryu, J. H.; Jang, C. J.; Yoo, Y. S.; Lim, S. G.; Lee, M. *J. Org. Chem.* **2005**, *70*, 8956–8962.

(29) Golubkov, G.; Weissman, H.; Shirman, E.; Wolf, S. G.; Pinkas, I.; Rybtchinski, B. *Angew. Chem., Int. Ed.* **2009**, *48*, 926–930.

(30) Krieg, E.; Shirman, E.; Weissman, H.; Shimoni, E.; Wolf, S. G.; Pinkas, I.; Rybtchinski, B. *J. Am. Chem. Soc.* **2009**, *131*, 14365–14373.

(31) Mulder, A.; Huskens, J.; Reinhoudt, D. N. *Org. Biomol. Chem.* **2004**, *2*, 3409–3424.

(32) Badjic, J. D.; Nelson, A.; Cantrill, S. J.; Turnbull, W. B.; Stoddart, J. F. *Acc. Chem. Res.* **2005**, *38*, 723–732.

(33) Würthner, F. *Chem. Commun.* **2004**, 1564–1579.

(34) Ahrens, M. J.; Sinks, L. E.; Rybtchinski, B.; Liu, W.; Jones, B. A.; Giaimo, J. M.; Gusev, A. V.; Goshe, A. J.; Tiede, D. M.; Wasielewski, M. R. *J. Am. Chem. Soc.* **2004**, *126*, 8284–8294.

(35) Cui, H.; Hodgdon, T. K.; Kaler, E. W.; Abezgauz, L.; Danino, D.; Lubovsky, M.; Talmon, Y.; Pochan, D. J. *Soft Matter* **2007**, *3*, 945–955.

(36) Friedrich, H.; Frederik, P. M.; de With, G.; Sommerdijk, N. A. J. M. *Angew. Chem., Int. Ed.* **2010**, *49*, 7850–7858.

(37) Shimizu, T.; Masuda, M.; Minamikawa, H. *Chem. Rev.* **2005**, *105*, 1401–1443.

(38) Wilson, T. M.; Zeidan, T. A.; Hariharan, M.; Lewis, F. D.; Wasielewski, M. R. *Angew. Chem., Int. Ed.* **2010**, *49*, 2385–2388.

(39) Svergun, D. I. *Biophys. J*. **1999**, *76*, 2879–2886.

(40) Svergun, D. I.; Koch, M. H. *Rep. Prog. Phys.* **2003**, *66*, 1735–1782.

(41) Smulders, M. M. J.; Nieuwenhuizen, M. M. L.; de Greef, T. F. A.; van der Schoot, P.; Schenning, A. P. H. J.; Meijer, E. W. *Chem.—Eur. J.* **2010**, *16*, 362–367.

(42) Smulders, M. M. J.; Schenning, A. P. H. J.; Meijer, E. W. *J. Am. Chem. Soc.* **2008**, *130*, 606–611.

(43) Martin, R. B. *Chem. Rev.* **1996**, *96*, 3043–3064.

(44) Zhao, D. H.; Moore, J. S. *Org. Biomol. Chem.* **2003**, *1*, 3471–3491.

(45) Smithrud, D. B.; Wyman, T. B.; Diederich, F. *J. Am. Chem. Soc.* **1991**, *113*, 5420–5426.

(46) Chandler, D. *Nature* **2005**, *437*, 640–647.

(47) Daniel, C.; Herz, L. M.; Silva, C.; Hoeben, F. J. M.; Jonkheijm, P.; Schenning, A. P. H. J.; Meijer, E. W. *Phys Rev B* **2003**, *68*, No. 235212.

(48) Fujitsuka, M.; Okada, A.; Tojo, S.; Takei, F.; Onitsuka, K.; Takahashi, S.; Majima, T. *J. Phys. Chem. B* **2004**, *108*, 11935–11941.

(49) Gilbert, E. E.; Voreck, W. E. *Propellants, Explos, Pyrotech.* **1989**, *14*, 19–23 and references therein.

(50) Lakowicz, J. R. *Principles of Fluorescence Spectroscopy*; Kluwer Academic/Plenum Publishers: New York, 1999.

(51) Petoukhov, M. V.; Konarev, P. V.; Kikhney, A. G.; Svergun, D. I. *J. Appl. Crystallogr.* **2007**, *40*, S223–S228.

(52) Wriggers, W.; Chacon, P. *J. Appl. Crystallogr.* **2001**, *34*, 773–776.

(53) Weissman, H.; Ustinov, A.; Shimoni, E.; Cohen, S. R.; Rybtchinski, B. *Polym. Adv. Technol.* **2011**, *22*, 133–138.

(54) Wallace, K. J.; Hanes, R.; Anslyn, E.; Morey, J.; Kilway, K. V.; Siegel, J. *Synthesis* **2005**, 2080–2083.